Title
Structural Basis for Sialoglycan Binding by the Streptococcus sanguinis SrpA Adhesin.

Journal
The Journal of biological chemistry, 291(14)

ISSN
0021-9258

Authors
Bensing, Barbara A
Loukachevitch, Lioudmila V
McCulloch, Kathryn M
et al.

Publication Date
2016-04-01

DOI
10.1074/jbc.m115.701425

Peer reviewed

THE JOURNAL OF BIOLOGICAL CHEMISTRY VOL. 291, NO. 14, pp. 7230–7240, April 1, 2016
Published in the U.S.A.

Structural Basis for Sialoglycan Binding by the *Streptococcus sanguinis* SrpA Adhesin*◆

Received for publication, November 16, 2015, and in revised form, January 5, 2016 Published, JBC Papers in Press, February 1, 2016, DOI 10.1074/jbc.M115.701425

Barbara A. Bensing[‡1], Lioudmila V. Loukachevitch[§1], Kathryn M. McCulloch[§1], Hai Yu[¶], Kendra R. Vann[‖], Zdzislaw Wawrzak[**], Spencer Anderson[**], Xi Chen[¶], Paul M. Sullam[‡], and T. M. Iverson[§‖‡‡§§2]

From the [‡]Division of Infectious Diseases, Veterans Affairs Medical Center, Department of Medicine, University of California, San Francisco and the Northern California Institute for Research and Education, San Francisco, California 94121, the Departments of [§]Pharmacology and [‖]Biochemistry, [‡‡]Center for Structural Biology, and [§§]Vanderbilt Institute of Chemical Biology, Vanderbilt University, Nashville, Tennessee 37232, the [¶]Department of Chemistry, University of California, Davis, California 95616, and [**]Life Sciences Collaborative Access Team, Synchrotron Research Center, Northwestern University, Argonne, Illinois 60439

***Streptococcus sanguinis* is a leading cause of infective endocarditis, a life-threatening infection of the cardiovascular system. An important interaction in the pathogenesis of infective endocarditis is attachment of the organisms to host platelets. *S. sanguinis* expresses a serine-rich repeat adhesin, SrpA, similar in sequence to platelet-binding adhesins associated with increased virulence in this disease. In this study, we determined the first crystal structure of the putative binding region of SrpA ($SrpA_{BR}$) both unliganded and in complex with a synthetic disaccharide ligand at 1.8 and 2.0 Å resolution, respectively. We identified a conserved Thr-Arg motif that orients the sialic acid moiety and is required for binding to platelet monolayers. Furthermore, we propose that sequence insertions in closely related family members contribute to the modulation of structural and functional properties, including the quaternary structure, the tertiary structure, and the ligand-binding site.**

Infective endocarditis is associated with significant morbidity and mortality (1). Although adherence between pathogen and host platelets is one of the first required steps for infection (2, 3), the pathogenesis of infective endocarditis is a complex process that is not well understood.

The viridans group of streptococci, including *Streptococcus sanguinis* and *Streptococcus gordonii*, accounts for an estimated 17–45% of all cases of infective endocarditis (4–6). These infective endocarditis-associated pathogens often contain a gene encoding a serine-rich repeat adhesin that can mediate the attachment of each respective pathogen to human platelet glycans (7–9). The adhesive interaction is perhaps best understood in *S. gordonii* strain M99, which interacts with platelets via the serine-rich repeat adhesin GspB. This surface component mediates host adherence via a binding region that promotes a high affinity interaction to a narrow range of sialylated carbohydrates (10). Studies using recombinant GspB and whole bacteria have shown that the binding of GspB to the sialylated glycans of GPIbα is the primary adhesive interaction to host platelets (7, 9, 11) and that expression of GspB enhances virulence (12).

S. sanguinis is often cited as the most common cause of bacterial infective endocarditis and contains a sequence homolog of GspB (8). In *S. sanguinis* strain SK36, this homolog is called SrpA and includes a binding region (termed $SrpA_{BR}$) that is 32% identical and 46% similar to the corresponding region of GspB (termed $GspB_{BR}$), but is significantly shorter, suggesting that $GspB_{BR}$ contains an additional domain as compared with $SrpA_{BR}$. Experimental validation of a role for SrpA in virulence is less clear than it is for GspB. Targeted mutagenesis of SrpA and other possible adhesins of *S. sanguinis* indicated that the deletion of SrpA does not influence virulence in an animal model of infective endocarditis (13). However, the subsequent finding that individual deletion of every identified cell wall anchored protein in *S. sanguinis* had no significant influence on virulence suggests that *S. sanguinis* could have multiple adhesins that provide functional redundancy (13).

Like GspB, SrpA binds platelet glycoprotein GPIbα and can mediate binding to platelets *in vitro* (8). Unlike GspB, SrpA appears to have a wider range of glycan-binding partners, but quantification of binding between SrpA and defined sialoglycans suggests only weak interactions for the carbohydrates tested (10). Sialoglycan array data further indicate that although GspB strongly prefers the *N*-acetylneuraminic acid (Neu5Ac) form of sialic acid, SrpA has some preference for glycans containing the *N*-glycolylneuraminic acid (Neu5Gc) form of sialic acid (10), which is not present in humans. Nevertheless, SrpA binds human platelets with high affinity (8); thus it is possible that a high affinity human carbohydrate ligand for SrpA remains unidentified.

The naturally occurring range of carbohydrate binding properties of GspB and SrpA can offer insights into the adhesive

* This work was supported by the Department of Veterans Affairs, National Institutes of Health Grants AI41513 (to P. M. S.) and AI106987 (to T. M. I. and P. M. S.), American Heart Association Grant 14GRNT20390021 (to T. M. I.), National Institutes of Health Training Grant in Molecular Biophysics T32 GM008320 and Education Grant for the Initiative to Maximize Student Development R25 GM062459 (to K. R. V.), and National Institutes of Health Training Grant in Mechanisms of Vascular Disease T32 HL007751 (to K. M. M.). A portion of the experiments described here used the Vanderbilt PacVan robotic crystallization facility, which was supported by National Institutes of Health Grant S10 RR026915. The authors declare that they have no conflicts of interest with the contents of this article. The content is solely the responsibility of the authors and does not necessarily represent the official views of the National Institutes of Health.
◆ This article was selected as a Paper of the Week.
The atomic coordinates and structure factors (codes 5EQ2, 5EQ3, and 5EQ4) have been deposited in the Protein Data Bank (http://wwpdb.org/).
[1] These authors contributed equally to this work.
[2] To whom correspondence should be addressed. E-mail: tina.iverson@vanderbilt.edu.

properties important for endovascular infection and may allow broader conclusions to be drawn about carbohydrate binding in these related adhesins. In previous work, we determined the crystal structure of the carbohydrate-binding region of GspB (14, 15). This binding region (termed $GspB_{BR}$) contains three linearly arranged, independently folded domains termed the CnaA, Siglec, and Unique domains based upon their structural similarity to other proteins. The binding pocket for sialylated carbohydrates is located within the Siglec domain. Site-directed mutagenesis of residues in the GspB binding pocket identified residues critical for both carbohydrate binding and platelet binding, as well as for virulence in the setting of infective endocarditis (14).

Here, we determine the crystal structure of the SrpA carbohydrate-binding region ($SrpA_{BR}$), both alone and in complex with a Neu5Gc-based synthetic sialyl galactoside disaccharide, and we use mutagenesis to validate key residues important for platelet binding. We identified a Thr-Arg motif conserved across homologous carbohydrate-binding adhesins that may orient the sialic acid moiety of carbohydrate ligands. Together, our results suggest that a small number of short sequence insertions in closely related homologs influence the quaternary structure, the tertiary structure, and the binding pocket. The latter may contribute to the differences in carbohydrate affinity and binding spectrum between SrpA and GspB.

Experimental Procedures

Expression and Purification—A codon-optimized gene for *S. sanguinis* strain SK36 $SrpA_{BR}$ (encoding residues 240–453 of the full protein) was synthesized (DNA 2.0) and subcloned into the isopropyl 1-thio-β-D-galactopyranoside-inducible pSV278 vector (Vanderbilt University), which encodes a His_6-maltose-binding protein (MBP)[3] affinity tag at the N terminus followed by a thrombin cleavage site. Variants of $SrpA_{BR}$ were cloned into pGEX5X, which encodes an N-terminal GST tag followed by a factor Xa protease cleavage site. Wild type and variant $SrpA_{BR}$ were expressed using the same protocol in *Escherichia coli* BL21 Gold (*DE3*) in LB medium and 50 μg/ml kanamycin or 100 μg ampicilllin, as appropriate for each plasmid. The cells were first grown at 37 °C until an A_{600} ~0.5 was reached and then were cold shocked in an ice bath for 20 min. The cells were then moved to 18 °C, induced with 0.5 mM isopropyl 1-thio-β-D-galactopyranoside, and grown for 18 h. Cells were harvested by centrifugation for 15 min at 5000 × *g* at 4 °C and frozen at −20 °C before purification.

Each frozen pellet was resuspended in binding buffer (20 mM Tris, pH 7.5, 200 mM NaCl, 1 mM EDTA) containing 1 mM PMSF, 2 μg/ml leupeptin, 2 μg/ml pepstatin, 1 μg/ml DNase, and 1 μg/ml RNase. The resuspended cells were then lysed by sonication. The lysate was clarified by centrifugation at 15,000 × *g* for 45 min and filtered using a 0.45-μm filter. Purification was performed at 4 °C. For wild-type $SrpA_{BR}$, the His_6-MBP-$SrpA_{BR}$ fusion protein was first purified by affinity chromatography with an MBP-Trap column. The eluted protein was concentrated in a 10-kDa cutoff concentrator and exchanged into 20 mM Tris, pH 7.5, and 200 mM NaCl. The His_6-MBP affinity tag was then cleaved with 1 unit of thrombin per mg of protein and separated from $SrpA_{BR}$ by passing the cleavage products over the MBP-Trap column in binding buffer. Variant $SrpA_{BR}$ was first purified on a GST-Trap column and concentrated, and then the GST tag was cleaved with factor Xa protease. GST was selectively removed from the cleavage products by passage over the GST-Trap column. For both wild-type and variant protein, the protein aggregates and excess affinity tag were removed using a 24-ml Superdex S-200 size exclusion column in 20 mM Tris-HCl, pH 7.5, and 200 mM NaCl. For some protein preparations, separation of $SrpA_{BR}$ from the fusion tag required an additional iteration of either affinity or size exclusion chromatography. After purification, the protein was >95% pure as assessed by visual inspection of the protein separated by SDS-PAGE.

Binding to Platelet Monolayers—The $SrpA_{BR}$ variant gene sequences, along with BamHI and EcoRI linkers, were synthesized (Life Technologies, Inc.) and then cloned in pGEX5X. The presence of only the expected alteration was verified by DNA sequence analysis. The GST-$SrpA_{BR}$ fusion proteins were expressed and purified as described (10).

To assess $SrpA_{BR}$ binding to platelets, fresh human platelets were washed, fixed, and immobilized in 96-well plates as described (16). All subsequent binding steps were carried at out room temperature. To reduce nonspecific adherence, the wells were treated with 50 μl of a 1× casein solution (blocking reagent, Roche Applied Science) in Dulbecco's PBS (DPBS) for 1 h. The blocking solution was replaced with 50 μl of purified GST-$SrpA_{BR}$ wild-type or variant proteins (0.5 μM in 1× blocking solution). The plates were incubated for 1 h with vigorous rocking; wells were rinsed three times with 100 μl of DPBS, and 50 μl of a rabbit polyclonal anti-GST (Life Technologies, Inc.) diluted 1:500 in 1× blocking solution was added to each well. After 1 h, wells were rinsed three times with 100 μl of DPBS, and 50 μl of a peroxidase-conjugated anti-rabbit antibody (1:5000 dilution in DPBS) was added. After incubation for 1 h, wells were rinsed three times with 100 μl of DPBS, and 200 μl of a solution of 0.4 mg/ml *o*-phenylenediamine dihydrochloride (Sigma) was added. The absorbance at 450 nm was read after ~15 min. Results are reported as the mean ± S.D., with $n = 4$ for each protein tested.

Synthesis of a Sialyl Galactoside Disaccharide Ligand (Neu5Gcα2–3GalβOMe) for $SrpA_{BR}$—GalβOMe (50 mg, 0.26 mmol), *N*-glycolylmannosamine (91 mg, 0.38 mmol), sodium pyruvate (113 mg, 1.03 mmol), and CTP (217 mg, 0.38 mmol) were dissolved in Tris-HCl buffer (10 ml, 100 mM, pH 8.5) containing $MgCl_2$ (20 mM) and appropriate amounts of *Pasteurella multocida* sialic acid aldolase (3 mg), *Neisseria meningitidis* CMP-sialic acid synthetase (2 mg), and *Pasteurella multocida* sialyltransferase 1 M144D (2 mg). The reaction was carried out by incubating the reaction mixture in an incubator shaker at 37 °C for 12 h. The reaction was monitored by TLC (EtOAc/MeOH/H_2O/HOAc = 5:2:1:0.1, by volume) with *p*-anisaldehyde sugar staining and mass spectrometry. When an optimal yield was achieved, to the reaction mixture was added the same volume (10 ml) of 95% ethanol followed by incubation at 4 °C

[3] The abbreviations used are: MBP, maltose-binding protein; r.m.s., root mean square; DPBS, Dulbecco's PBS; GalβOMe, methyl β-galactopyranoside; ULI, unique loop insertion.

TABLE 1

Crystallographic data collection and refinement statistics

Values in parentheses are for the highest resolution shell. The osmium derivative was used for phasing and was not refined. NA means not applicable.

	$SrpA_{BR}$	$SrpA_{BR}$ (Os)	$SrpA_{BR}$ Neu5Gcα2–3GalβOMe	$SrpA_{BR}$ R347E
PDB entry	5EQ2	NA	5EQ3	5EQ4
Data collection				
Beamline	ID-F	ID-D	ID-G	ID-G
Wavelength	0.979 Å	1.13966 Å	0.979 Å	0.979 Å
Space group	C2	C2	C2	$P2_12_12_1$
Unit cell	a = 174.5 Å b = 46.8 Å c = 64.8 Å β = 102.7°	a = 174.4 Å b = 46.8 Å c = 64.7 Å β = 102.8°	a = 174.6 Å b = 47.0 Å c = 64.0 Å β = 102.2°	a = 44.7 Å b = 88.1 Å c = 199.2 Å
Resolution	1.8 Å	2.2 Å	2.0 Å	2.3 Å
R_{sym}	0.061 (0.450)	0.101 (0.467)	0.131 (0.500)	0.095 (0.563)
R_{pim}	0.034 (0.244)	0.029 (0.188)	0.054 (0.224)	0.045 (0.316)
I/σ	30.9 (4.8)	34.1 (5.1)	23.0 (2.9)	14.2 (2.2)
Completeness (%)	98.8 (100)	100 (100)	94.7 (78.0)	91.8 (71.6)
Redundancy	4.0 (4.2)	12.5 (7.0)	6.8 (5.3)	4.8 (3.6)
$CC_{1/2}$	0.960	0.935	0.881	0.759
Refinement				
No. of molecules/asymmetric unit	2		2	4
R_{cryst}	0.178		0.198	0.202
R_{free}	0.208		0.243	0.257
r.m.s. deviation				
Bond lengths	0.01 Å		0.007 Å	0.002 Å
Bond angles	1.15°		0.98°	0.59°
Ramachandran				
Favored	97.7%		96.8%	96.6%
Allowed	2.3%		3.2%	3.1%
Outliers	0%		0%	0.3%
Average B-factor	31.54 Å^2		35.21 Å^2	30.94 Å^2
Ligand B-factor	—		42.58 Å^2	

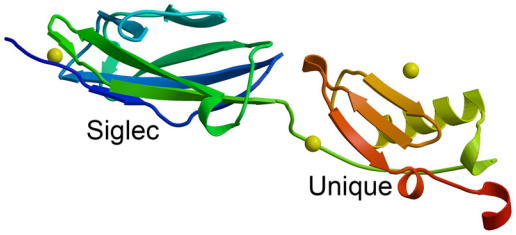

FIGURE 1. **Structure of the $SrpA_{BR}$ protomer.** Ribbons diagram of $SrpA_{BR}$ protomer colored by sequence with the N terminus in *blue* and the C terminus in *red*. Assigned Ca^{2+} ions are shown as *yellow spheres*.

for 30 min. The precipitates were removed by centrifugation (5533 × *g*, 30 min), and the supernatant was concentrated and purified by Bio-Gel P-2 gel filtration chromatography (water was used as an eluent). Further purification was achieved using silica gel chromatography (EtOAc/MeOH/H_2O = 4:2:1, by volume) and a final pass through of a Bio-Gel P-2 gel filtration column to produce Neu5Gcα2–3GalβOMe (101 mg). Yield, 81%; white foam. ^{1}H NMR (800 MHz, D_2O) δ 4.38 (d, J = 8.0 Hz, 1H), 4.10 (s, 2H), 4.08 (dd, J = 9.6 and 3.2 Hz, 1H), 3.93 (d, J = 2.8 Hz, 1H), 3.91 (t, J = 10.4 Hz, 1H), 3.86–3.58 (m, 10H), 3.56 (s, 3H), 3.53 (t, J = 8.8 Hz, 1H), 2.75 (dd, J = 12.8 and 4.8 Hz, 1H), 1.79 (t, 1H, J = 12.0 Hz, 1H); ^{13}C NMR (200 MHz, D_2O) δ 175.66, 173.76, 103.34, 99.70, 75.72, 74.81, 73.43, 72.44, 71.73, 69.02, 67.96, 67.85, 67.40, 62.38, 60.84, 56.91, 51.25, 39.60; high resolution mass spectrometry (ESI) *m/z* calculated for $C_{18}H_{30}O_{15}N$ (M − H) 500.1615, found 500.1608.

Crystallization, Data Collection, Structure Determination, Refinement, and Analysis—$SrpA_{BR}$ was concentrated and buffer exchanged into 20 mM Tris-HCl, pH 7.2. All crystals grew using the sitting drop vapor diffusion method in a CombiClover 4 chamber plate at room temperature (~23 °C) by equilibrating droplets containing 1 μl of protein and 1 μl of reservoir solution over 50 μl of a reservoir solution. Native crystals grew in space group C2 using a protein concentration of 10.6 mg/ml and a reservoir condition that contained 0.2 M $Ca(CH_3CO_2)_2$, 0.1 M sodium cacodylate, pH 6.5, and 18% PEG 8000. Cocrystals of $SrpA_{BR}$ with the Neu5Gcα2–3GalβOMe synthetic disaccharide used 14.4 mg/ml protein in a buffer solution containing 10 mM carbohydrate and 20 mM Tris-HCl, pH 7.2. Crystals of the $SrpA_{BR}$ R347E variant were grown using a protein concentration of 15.3 mg/ml and a reservoir solution containing 0.2 M $NaCH_3COO$, 0.1 M sodium cacodylate, pH 6.5, and 30% PEG 8000. An Os derivative was generated by soaking fully formed crystals in the C2 space group in reservoir solution supplemented with 2 mM K_2OsO_4 and 5% DMSO overnight. Native crystals were cryo-protected using a solution containing all of the components of the reservoir solution plus 5% DMSO before cryo-cooling while the Os derivative crystals were flash-cooled directly from the soaking drop, and disaccharide cocrystals were cryo-cooled using the well solution supplemented with 5 mM disaccharide. Diffraction data were collected using the LS-CAT beamlines of the Advanced Photon Source at −180 °C as listed in Table 1. Data were processed using the HKL2000 (17) and CCP4 (18) suites of programs.

The structure in the C2 space group was determined using single wavelength anomalous diffraction phasing from the Os derivative. Eleven Os sites were identified using the AutoSol subroutine in Phenix (19, 20), and phases were calculated using a f'' of 10.2 and an f' of −17.65 with an overall figure of merit of 0.221. Phases were improved using the Resolve subroutine in Phenix (19), and the initial model was built using the Buccaneer subroutine in Phenix (19, 21). This procedure identified two molecules in the asymmetric unit and resulted in a model with

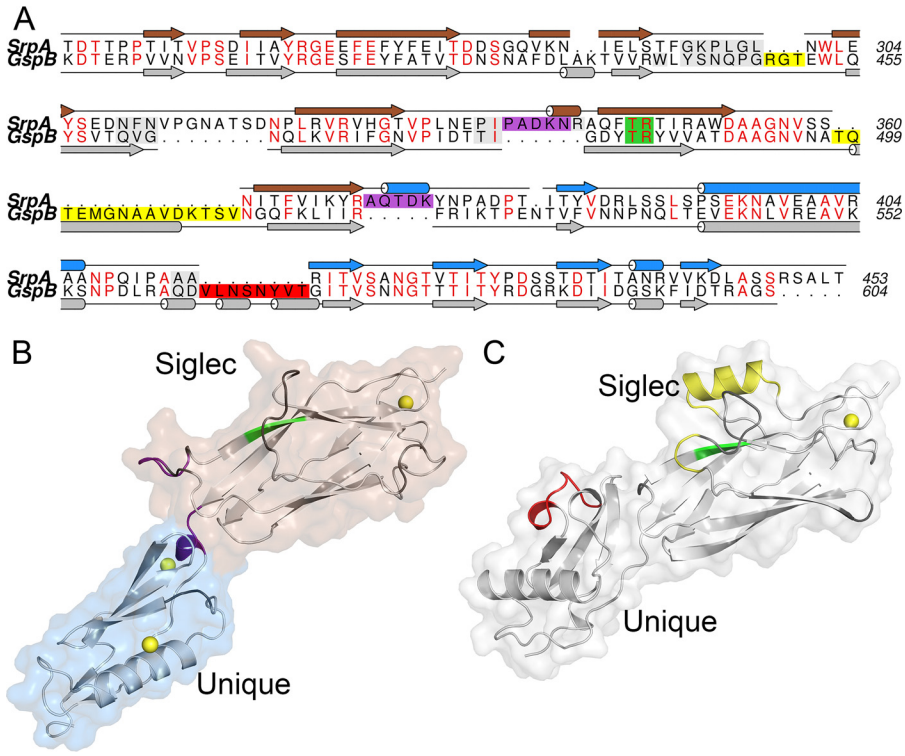

FIGURE 2. **Structure-based sequence alignment of SrpA and GspB.** *A,* sequence alignment was performed manually by overlaying the structures of $SrpA_{BR}$ and $GspB_{BR}$. Secondary structural elements are shown above and below the sequence. Amino acids in *red text* are identical. The Thr-Arg motif is highlighted in *green*. The insertions in GspB highlighted in *yellow* are near the ligand binding pocket, with residues 449–451 forming a short loop and residues 498–514 forming the helix at the carbohydrate binding pocket. Insertions in SrpA highlighted in *purple* are predicted to influence the interdomain angle, and the insertion in GspB highlighted in *red* is predicted to prevent dimerization. *B,* ribbon diagram of $SrpA_{BR}$ with sequence inserts and binding site residues colored according to the sequence alignment and superimposed onto a surface where the Siglec domain is *brown* and the Unique domain is *blue*. *C,* ribbon diagram of the $GspB_{BR}$ Siglec and Unique domains with sequence inserts and binding site residues colored according to the sequence alignment and superimposed onto a surface of the binding region.

an R_{free} of 0.24. The initial coordinates then transferred directly into the native data set with an initial round of rigid body refinement.

The unliganded and disaccharide-bound crystals of $SrpA_{BR}$ were isomorphous, and thus the disaccharide-bound structure was determined by isomorphous replacement. In short, following refinement of the unliganded structure, all solvent molecules were removed, and the coordinates were transferred directly into the dataset for $SrpA_{BR}$ cocrystallized with the disaccharide. The coordinates were subjected to rigid body refinement in Phenix (19), resulting in an initial R_{free} of 0.27. Unambiguous electron density for the sialic acid was observed even in the initial electron density maps, and both the sialic acid and the galactose were placed into the model after two rounds of refinement. The occupancy of the disaccharide was retained at 1.0 for the duration of the refinement, and the average temperature factors of this ligand (42.6 $Å^2$) are similar to that of the protein (35.2 $Å^2$) in the final model.

The structure of the R347E variant in the $P2_12_12_1$ space group was determined by molecular replacement using the Phaser subroutine in Phenix and the coordinates of the unliganded protein with all solvent molecules and ligands removed. The final model of the R347E variant contained a geometric outlier (Table 1) within the loop that changed position upon mutation. This region contains electron density that was challenging to assign with confidence.

All models were improved with iterative rounds of model building in Coot (22) and refinement in Phenix (19). Domain rotation analysis was performed using the DynDoM web server (23).

Dynamic Light Scattering—Dynamic light scattering was performed using a DynaPro NanoStar instrument (Wyatt Technology) on protein samples that were first filtered through a 0.22-μm Spin-X centrifugal filter (Corning Inc.). Measurements were performed in triplicate with an $SrpA_{BR}$ concentration of 1 mg/ml in 20 mM sodium cacodylate, 10 mM $CaCl_2$, pH 7.2, at 25 °C. Three measurements of 10 acquisitions were collected for each of three $SrpA_{BR}$ samples. Dynamics 7.1.9 software was used for data analysis.

Results

Structure of $SrpA_{BR}$—The x-ray crystal structure of unliganded $SrpA_{BR}$ (residues 240–453 of the full-length protein) was determined to 1.8 Å resolution (Table 1) using *de novo* phasing calculated from single wavelength anomalous diffraction of an osmium derivative. Each $SrpA_{BR}$ protomer folds into two domains (Fig. 1). The N-terminal domain is similar to the "Siglec"-like domain of GspB that is a variant of a V-set Ig fold, with an r.m.s. deviation of 1.8 Å over the 102 amino acids in the alignment. The C-terminal domain is similar to the "Unique" domain of GspB with an r.m.s. deviation of 1.4 Å over the 76 amino acids in the alignment. Given the close conservation of

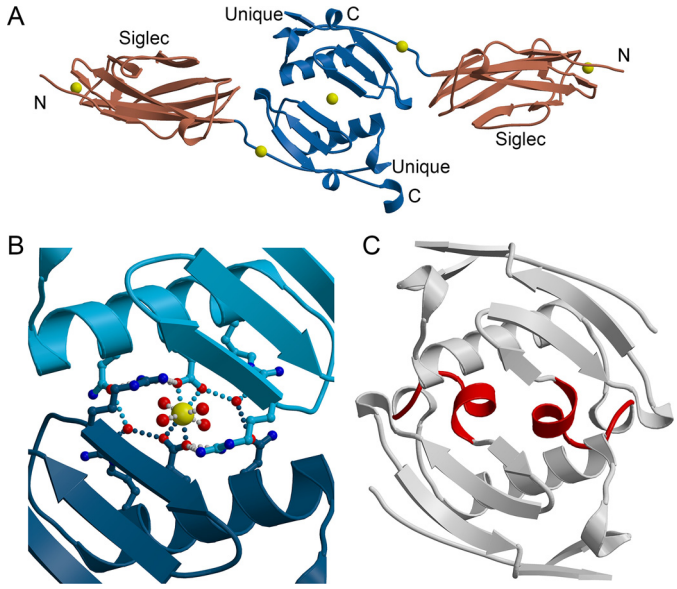

FIGURE 3. **Structure of the $SrpA_{BR}$ dimer.** *A,* ribbon diagram of the crystallographic asymmetric unit containing the $SrpA_{BR}$ dimer colored by domain. The N-terminal Siglec domains are shown in *brown,* and the C-terminal Unique domains are shown in *blue.* Electron density assigned as Ca^{2+} ions are shown as *yellow spheres*. The view is down the non-crystallographic 2-fold axis of symmetry. *B,* view of the Ca^{2+} ion mediating dimerization between the Unique domains. Side chains involved in a hydrogen-bonding network that contributes to Ca^{2+} coordination are *highlighted*. The view is the same as in *A*. *C,* modeling of the GspBUnique domain (*gray*) into the same orientation as the SrpA Unique domain dimer identifies a sequence insertion of seven amino acids (residues 564–571; *red*) that sterically prevents oligomerization in the same manner as is observed in the $SrpA_{BR}$ crystal structure.

fold in each domain, we used these structures to improve the accuracy of our sequence alignment with GspB (Fig. 2). This sequence alignment reveals several notable insertions in each adhesin with respect to each other. These insertions add structural elements to the surface of SrpA (Fig. 2*B*) or GspB (Fig. 2*C*) that appear to alter the structural and functional properties of the adhesins.

One major difference between SrpA and GspB is the oligomerization state. The arrangement of $SrpA_{BR}$ in the crystal suggests that this adhesin forms antiparallel dimers mediated by the C-terminal Unique domain (Fig. 3*A*). This mode of dimerization buries 1535 Å^2 of surface area per protomer, includes a Ca^{2+}-mediated interaction, and contains both hydrogen bonding and hydrophobic interactions (Fig. 3*B*). Both the amount of buried surface area and the nature of the contacts were consistent with what was anticipated for a physiological dimer. To suggest a possible structural basis for $SrpA_{BR}$ dimerization when the homologous $GspB_{BR}$ is a monomer, we superimposed the dimer interface of $SrpA_{BR}$ with the equivalent region of the $GspB_{BR}$ structure. This structural comparison identified a short insertion of eight amino acids in $GspB_{BR}$ (residues 564–571, *red*; Fig. 2) as compared with $SrpA_{BR}$ that would sterically prevent dimerization (Fig. 3*C*). To date, most characterized serine-rich repeat adhesins have been demonstrated as structural and functional monomers (14, 24–27), although a domain-swapped dimer is observed in the keratin-binding adhesin KRT4 from *Streptococcus agalactiae* (28). Thus, we assessed whether the dimer observed in the crystal structure was present in solution using dynamic light scattering. The $SrpA_{BR}$ protein was monodisperse, and we measured a peak molecular mass of 43.9 ± 3.6 kDa using this technique (Table 2). This value is consistent with the theoretical molecular mass of a $SrpA_{BR}$ dimer of 46.8 kDa. We then constructed two variants of $SrpA_{BR}$ predicted to influence dimerization. The first mutation is a charge reversal of the Glu-400 side chain (E400R) that is predicted to disrupt dimerization through loss of Ca^{2+} coordination. The second variant incorporates the eight-amino acid insertion of the GspB Unique domain into the equivalent position of the SrpA Unique domain. This unique loop insertion (ULI) is predicted to disrupt dimerization sterically. Dynamic light scattering of the E400R variant had a calculated molecular mass of 33.2 ± 1.27 or half-way between monomer and dimer (Table 2). The E400R variant was associated with a significant increase in polydispersity (Table 2), suggesting that the presence of both the dimeric and monomeric forms in solution is possible for this variant. The ULI variant was associated with low heterologous expression levels in *E. coli*. Moreover, significant protein loss during purification resulted in sample quantity and purity being insufficient for accurate measurements by dynamic light scattering (data not shown).

A second major difference in the structures of GspB and SrpA is the orientation of the Siglec and Unique domains with respect to each other (Fig. 4). A domain rotation of 101° would be required to allow both domains of $SrpA_{BR}$ and $GspB_{BR}$ to overlay with each other. Close analysis of the structures indicates that the domains of SrpA are unlikely to adopt the same interdomain orientations as are observed in the GspB structure, even allowing for interdomain flexibility. Manual rotation of the SrpA Siglec and Unique domains into the orientations observed in GspB identifies two short sequence insertions between the secondary structural elements of $SrpA_{BR}$ (residues 335–342 and residues 373–376, *purple*; Figs. 2 and 4) that would result in significant steric clashes if the domains of SrpA adopted the same interdomain angle as found between the domains of GspB. Thus, despite high overall sequence and structural similarity of each individual domain, these two small sequence insertions likely result in dramatic differences in the tertiary structure of the SrpA- and GspB-binding regions.

Carbohydrate Binding Properties of $SrpA_{BR}$—To assess how carbohydrate binds to SrpA, we synthesized a Neu5Gc-based sialyl galactoside disaccharide (Neu5Gcα2–3GalβOMe) for use in crystallization. We selected this disaccharide for its similarity to the higher affinity ligands of SrpA (10). The disaccharide was synthesized from GalβOMe and *N*-glycolylmannosamine using a highly efficient one-pot three-enzyme sialylation system (29, 30) containing *Pasteurella multocida* sialic acid aldolase (31), *Neisseria meningitidis* CMP-sialic acid synthetase (32), and *P. multocida* sialyltransferase 1 M144D mutant (33). A yield of 81% was achieved after purification.

The location and architectural details of the carbohydrate-binding site in $SrpA_{BR}$ were identified by cocrystallizing $SrpA_{BR}$ with the synthetic Neu5Gcα2–3GalβOMe disaccharide. The cocrystals diffracted to 2.0 Å resolution (Table 1), and following initial isomorphous replacement with the unliganded $SrpA_{BR}$ structure, unambiguous electron density for the sialic acid moiety of the disaccharide was readily apparent in one of the two molecules of the dimer. Electron density consistent with the

TABLE 2
Dynamic light scattering of $SrpA_{BR}$
ND means not determined. This light scattering measurement was identified as multimodal by the Dynamics Version 7.1.9 software, which prevented a numerical calculation of % polydispersity.

Sample	Poly-dispersity	Sum of squares	Amplitude	Baseline	Peak radius	Peak mass ratio
	%				nm	kDa
$SrpA_{BR}$-1	13.6	5.344	0.269	1.001	3.1	48.0
$SrpA_{BR}$-2	14.5	9.048	0.273	1.001	2.9	42.1
$SrpA_{BR}$-3	12.8	5.077	0.251	1.001	2.9	41.5
Mean						43.9
S.D.						3.6
E400R-1	26.9	10.368	0.234	1.003	2.7	33.8
E400R-2	ND	34.709	0.220	1.006	2.7	34.0
E400R-3	28.3	14.354	0.227	1.005	2.6	31.7
Mean						33.2
S.D.						1.27

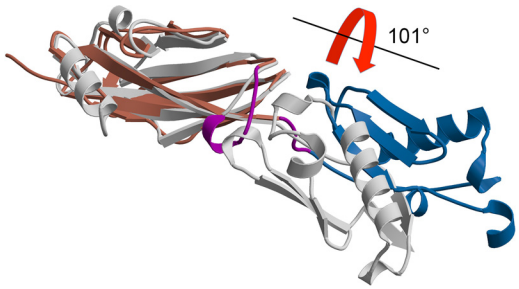

FIGURE 4. **Domain orientation of the $SrpA_{BR}$ protomer comparison of the $SrpA_{BR}$ Siglec and Unique domains (*brown* and *blue*) to the $GspB_{BR}$ domains (*gray*) highlights the difference in interdomain angle between the two structures.** Two sequence insertions in SrpA (residues 335–342 and residues 373–376; *magenta*) as compared with GspB prevent these two homologs from adopting the same interdomain orientation. Ca^{2+} ions are omitted for clarity.

galactoside appeared after a single round of refinement, although this electron density was not as clear as the density for the sialic acid (Fig. 5, *A* and *B*). Unambiguous electron density for the disaccharide never appeared in the second molecule of the dimer. Instead, the second nominally unoccupied pocket in the dimer contains diffuse electron density that could not be assigned with confidence, suggesting that this location may be interacting with components from the crystallization reservoir. Inspection of the crystal lattice suggests that the lack of ligand binding to the second protomer results from crystal packing interactions. Specifically, the C terminus of one protomer partially occupies the carbohydrate-binding pocket, likely displacing the ligand. The r.m.s. deviation between liganded and unliganded forms of the protein was 0.3 Å over 197 Cα atoms, indicating that there is not a significant global conformational change upon carbohydrate binding. Moreover, an overlay of the Cα atoms of the regions surrounding the carbohydrate binding pocket is associated with an r.m.s. deviation of 0.24 Å, indicating that there are no significant local conformational differences that accompany carbohydrate binding.

The glycan-binding site of $SrpA_{BR}$ is located along an edge β-strand of the Siglec domain and shows significant structural differences when compared with that observed in the structure of $GspB_{BR}$ (Fig. 5, *B* and *C*). Most strikingly, the $SrpA_{BR}$-binding site appears to be shallow, solvent-exposed, and relatively featureless from a topographic perspective (Fig. 6*A*). In contrast, the structurally equivalent region in $GspB_{BR}$ is hallmarked by a defined and complex groove (Fig. 6*B*) that is likely incompatible with all but a few conformations of sialylated trisaccharides, but it could provide numerous stabilizing contacts for a ligand with the correct glycan composition and geometry. This architectural difference is consistent with the demonstrated differences in binding affinities and binding spectra between the two adhesins, with SrpA having a low affinity and broad selectivity, and GspB having a high affinity and narrow selectivity (10). Interestingly, two short sequence insertions in GspB (residues 449–451 and residues 498–514, *yellow*, Fig. 2) as compared with SrpA are near the GspB binding groove and promote dramatic remodeling of the region predicted to interact with the third sugar of a trisaccharide.

Examination of the interactions between $SrpA_{BR}$ and the disaccharide only identifies specific contacts to the sialic acid moiety. Direct contacts include interactions with the Arg-342 backbone carbonyl, the Gln-344 backbone carbonyl, the Tyr-368 side chain OH, the Thr-346 amide nitrogen and side chain Oγ, and the Arg-347 side chain Nη1 and Nη2 (Fig. 6*C*). Of these, the Tyr-368 side chain hydroxyl forms a hydrogen bonding interaction to the O11 hydroxyl of Neu5Gc, an atom unique to Neu5Gc. Interestingly, the sequence insertion between residues 335 and 342 (SrpA numbering) alters the orientation of Tyr-368 as compared with Ile-520 of GspB such that the side chain hydroxyl is optimally aligned for this hydrogen-bonding interaction, suggesting a dual purpose for this particular sequence insertion.

The four interactions of Thr-346 and Arg-347 to both oxygen atoms of the carboxylate at the C1- (Thr-346) and the C8- and C9-hydroxyl groups (Arg-347) of the sialic acid appear to define the binding orientation of the sialic acid. Notably, these two residues appear to be absolutely conserved in the Siglec domains of all serine-rich repeat adhesins demonstrated to bind sialylglycans (Ref. 10 and data not shown). Moreover, these side chains appear to adopt identical conformations in the structures of both $SrpA_{BR}$ and $GspB_{BR}$ (Thr-483 and Arg-484). Taken together, the structural studies suggest that these residues may anchor and orient the sialic acid in sialic-binding serine-rich repeat homologs.

Manual Docking of Disaccharide in $GspB_{BR}$—We next used the structural alignment of the Siglec domains of $SrpA_{BR}$ and $GspB_{BR}$ (39% identical, with an r.m.s. deviation of 1.8 Å over 102 aligned residues; Protein Data Bank code 3QC5 (14)) to explain how the conserved Thr-Arg motif may orient the sialic acid moiety of the Neu5Gc- or Neu5Ac-containing disaccharides. The position of the Neu5Gc extrapolated from the coor-

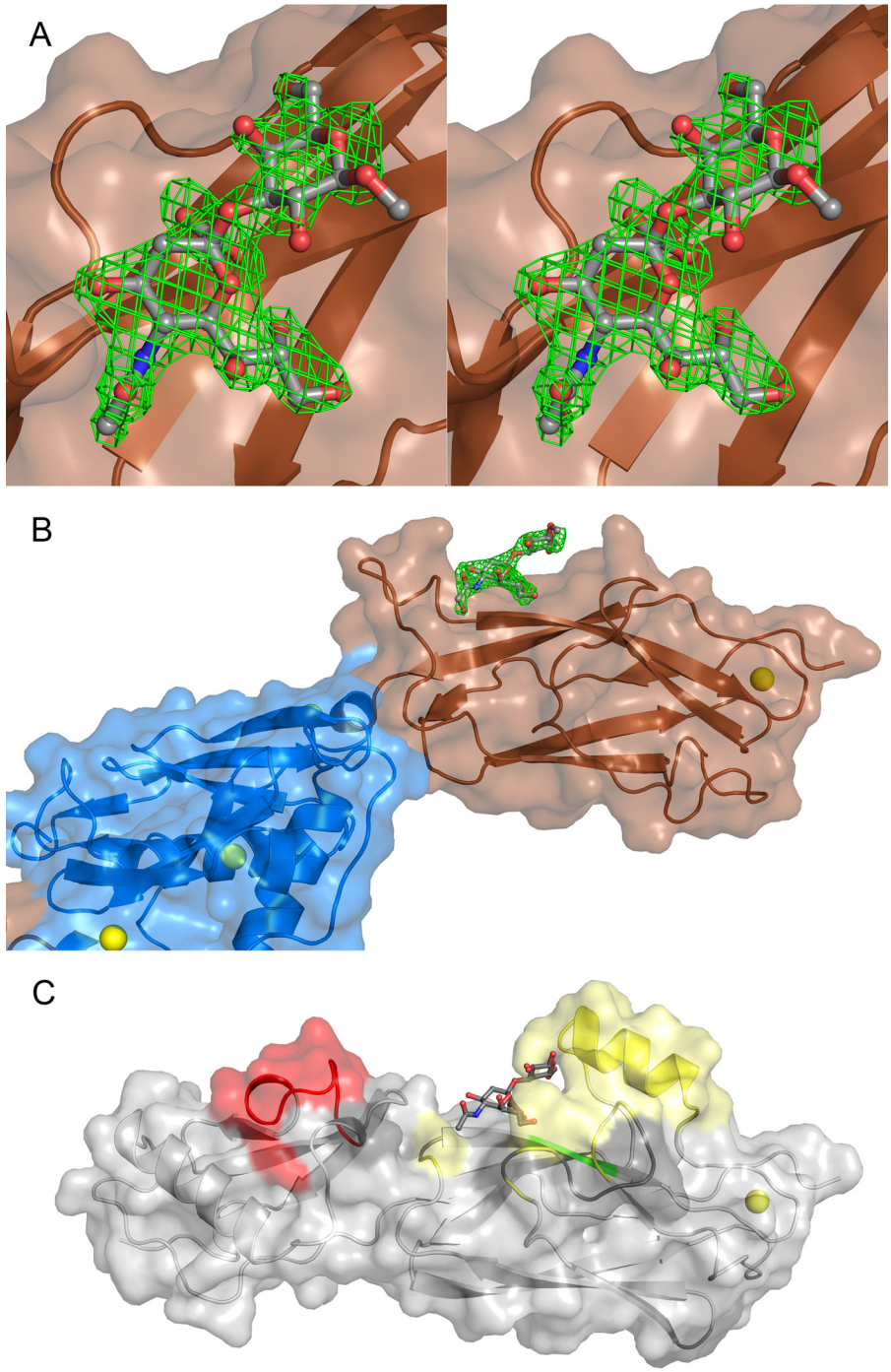

FIGURE 5. **Carbohydrate binding in $SrpA_{BR}$.** *A* and *B* are superimposed with $|F_o| - |F_c|$ difference electron density contoured at 3σ and calculated after removal of the ligand and refinement in Phenix. *A,* stereoview of the sialyl galactoside disaccharide bound to $SrpA_{BR}$ highlights the quality of the electron density map. *B,* surface representation of $SrpA_{BR}$ focusing on one protomer of the dimer. The Siglec domain is colored in *brown,* and the Unique domain is colored in *blue*. The view highlights large and open binding pocket for carbohydrate ligand. *C,* surface representation of $GspB_{BR}$ with the same orientation of the carbohydrate-binding Siglec domain as $SrpA_{BR}$ in *B*. The sequence inserts of $GspB_{BR}$ with respect to $SrpA_{BR}$ are colored using the same coloring scheme as is used in Fig. 2. To mark the global location of the ligand binding pocket, a Neu5Acα2–3Gal disaccharide is modeled using the position from $SrpA_{BR}$; however, its position is not experimentally determined.

dinates of disaccharide experimentally identified in $SrpA_{BR}$ was used as a guide to manually position a Neu5Ac-containing sialyl galactoside disaccharide in the $GspB_{BR}$ binding pocket adjacent to the Thr-483 and Arg-484 of the Thr-Arg motif. We used this model to assess potential bonding interactions between $GspB_{BR}$ and the sialoglycan. In this model, the Thr-Arg motif maintains four hydrogen bonds to the sialic acid moiety. Additional polar residues within 4 Å of the docked disaccharide include Tyr-443, Arg-449, Thr-478, Tyr-482, Lys-509, and Arg-585. In addition, the side chain of Tyr-485 lines the region where the third glycan of a trisaccharide is expected to bind if this docking is correct. Notably, Arg-449 and Lys-509 are part of the insertions in $GspB_{BR}$ that help remodel the binding site (*yellow*, Fig. 2).

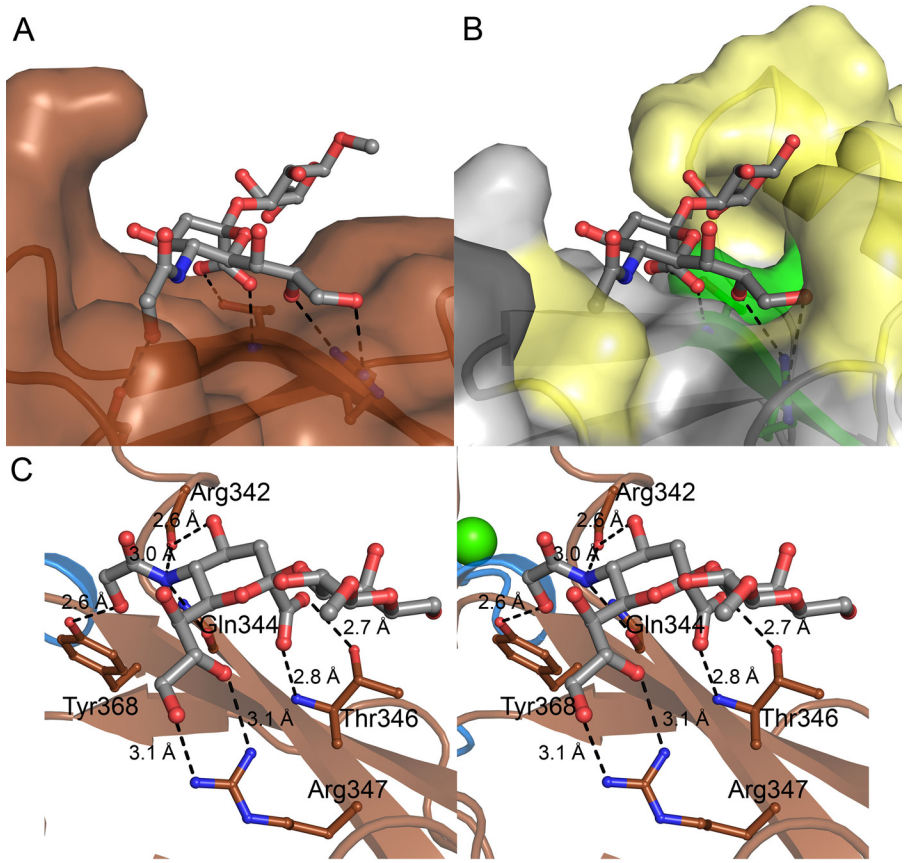

FIGURE 6. **Role of the Thr-Arg motif in orienting carbohydrate ligand.** *A* and *B*, zoomed in view of the Neu5Gcα2–3GalβOMe sialyl galactoside disaccharide-binding site of $SrpA_{BR}$ (shown as *sticks*) in the context of the binding pocket (shown as a surface). *A*, $SrpA_{BR}$, the disaccharide position is experimentally determined; *B*, $GspB_{BR}$, the disaccharide is modeled based upon the Thr-Arg motif and is not experimentally determined. The view highlights the conservation of the hydrogen bond locations provided by the Thr-Arg motif and the more restricted binding pocket of $GspB_{BR}$ that likely restricts the range of carbohydrates that can bind. *C*, stereoview of sialyl galactoside in the binding site of $SrpA_{BR}$. Distances consistent with hydrogen bonding interactions are shown as *dotted lines*.

Role of Structural Properties in Platelet Binding—We combined site-directed mutagenesis with binding measurements to assess how the structural properties of SrpA influence binding to human platelet monolayers. We tested two types of variants. We first assessed how amino acids directly interacting with the sialic acid group influenced platelet binding using the T346V and R347E variants. We also tested the influence of dimerization on the binding to platelet monolayers using the E400R and the ULI variants. $SrpA_{BR}$ variants with altered residues within the binding pocket had dramatically reduced binding to platelet monolayers, whereas mutations designed to disrupt dimerization had platelet binding statistically similar to wild type (Fig. 7*A*).

Mutations of amino acids on the surface of a protein rarely perturb the global structure of a protein. To ensure that mutations of $SrpA_{BR}$ that exhibit reduced binding do not impact folding, we selected the R347E variant, as the charge reversal would be the more likely to be disruptive to the global structure, and determined the structure.

The crystals of the $SrpA_{BR}$-R347E variant grew under modified chemical conditions as compared with wild-type $SrpA_{BR}$ and were a primitive orthorhombic crystal form as compared with the monoclinic crystal form of the wild-type protein (Table 1). The structure of the $SrpA_{BR}$-R347E variant retains the anticipated global fold. Despite retention of all secondary structural elements, the two loops that surround the sialic acid binding pocket undergo conformational rearrangement upon mutation. These loops include residues 292–300 and 338–342 and have a maximal displacement of 10 Å (Fig. 7*B*) that collapses the carbohydrate-binding site somewhat. However, the electron density for these shifted regions is of poor quality. Indeed, for one protomer in the unit cell, the chain could not be modeled with confidence and was therefore omitted from the coordinates. There were additional structural changes outside of these loop regions that are anticipated to result both from differences in crystal packing upon the change in space group and from the change in crystallization conditions (specifically, the lack of Ca^{2+}, which binds at several sites in $SrpA_{BR}$ and mediates dimerization). Nevertheless, this crystal structure confirms that R347E substitution does not result in global protein misfolding.

Discussion

Molecular Mechanism for Tuning Functional Properties in Lectin-like Serine-rich Repeat Adhesins—A comparison of the structures of $SrpA_{BR}$ and $GspB_{BR}$ identifies that some of the major structural and functional differences in these related proteins are likely influenced by short sequence insertions (3–16 amino acids) between the secondary structural elements (Fig.

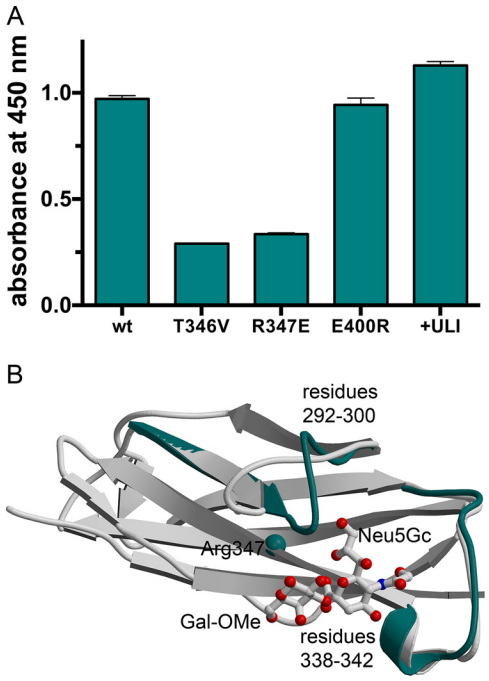

FIGURE 7. **Validation of the ligand binding pocket by mutagenesis.** *A,* binding of wild-type and variant SrpA to platelet monolayers. ULI indicates the inclusion of seven amino acids of the GspB Unique domain into the equivalent position on the SrpA Unique domain. *B,* overlay of the Siglec domain of the disaccharide-bound wild-type $SrpA_{BR}$ (*gray*) with regions of the $SrpA_{BR}$ R347E variant that exhibited conformational difference (*teal*). The comparison identifies significant differences of positions between the two loops that sterically occlude the sialic acid binding pocket in the R347E variant. The location of the Cα atom of Arg-347 is indicated with a *cyan sphere*.

2). Three features of $SrpA_{BR}$ and $GspB_{BR}$ appear to be tuned by such a mechanism.

The first feature influenced by sequence inserts is dimerization. The $SrpA_{BR}$ dimer is reproduced both in solution, as monitored by dynamic light scattering (Table 2), and in a crystal (Fig. 3*A*). Dimerization is mediated by the Unique domain in SrpA; however, a sequence insertion of seven amino acids in GspB is predicted to sterically prevent a similar interaction (Fig. 3*C*). Disruption of dimerization via substitution of a Ca^{2+}-binding residue or insertion of the unique loop of GspB into SrpA does not strongly affect glycan binding (Table 2 and Fig. 7). This result is consistent with our previous finding that Ca^{2+} is not required for SrpA binding to sialoglycans (10). Thus, the physiological relevance of Ca^{2+} binding and dimerization is not clear at this time.

A second feature that appears to be modulated by a sequence insertion is interdomain orientation within the protomer. Here, two insertions (seven amino acids and three amino acids, respectively) in SrpA as compared with GspB dramatically alter the interactions between domains, which likely changes the interdomain angle (Fig. 4). One functional consequence of this domain reorganization is the alteration of residues at the periphery of the sialoglycan binding pocket. Specifically, the insert between residues 335 and 342, which appears to promote domain orientation, also allows the side chain of Tyr-368 to orient toward the sialoglycan binding pocket.

Finally, the shape of the ligand-binding site is altered by insertions in GspB as compared with SrpA. These insertions in GspB result in a binding pocket with a deep groove that may both allow a greater number of interactions between the carbohydrate and the adhesin and simultaneously sequester ligand from solvent (Fig. 5). Both of these consequences are predicted to increase the carbohydrate affinity and narrow the sialoglycan binding spectrum in GspB as compared with SrpA. This prediction is consistent with the observed difference in affinity and selectivity demonstrated for these two adhesins (10).

Sequence Motif for Sialic Acid Recognition in Siglec-containing Adhesins—The serine-rich repeat family of adhesins is an expanding family of virulence factors. A question in the field is how closely related homologs recognize sialoglycans but have significantly different selectivity. The identification of the Thr-Arg sequence in $SrpA_{BR}$, the conservation of this motif in homologous sialoglycan-binding adhesins (Ref. 10 and data not shown), and the close maintenance of the geometry of the Thr-Arg side chains between $SrpA_{BR}$ and $GspB_{BR}$ (14) all support the Thr-Arg motif as a previously unrecognized sialic acid-binding motif for this family. Supporting this proposal is our observed loss of platelet binding by variants that substituted Thr-346 and Arg-347 of SrpA (Fig. 7*A*). The Thr-Arg motif of SrpA (Thr-346–Arg-347) is equivalent to Thr-483-Arg–484 of GspB (Fig. 2). Consistent with our findings here, previous work on GspB shows that mutation of Arg-484 reduces glycan binding, platelet binding, and virulence in an animal model of endocarditis (14).

We thus applied our analysis of the $SrpA_{BR}$ structure with disaccharide bound (Fig. 5, *A* and *B*) to the $GspB_{BR}$ structure by manually docking a Neu5Ac-containing sialyl galactoside disaccharide into the $GspB_{BR}$ binding pocket. In this model, the sialic acid moiety is predicted to maintain four hydrogen bonding interactions with Thr-483 and Arg-484, and there are no clashes between the docked ligand and the protein (Fig. 5*C*). Moreover, this docking suggests that disaccharide would likely form hydrogen bonding contacts to GspB residue Tyr-443 (among other residues), whereas trisaccharide would likely form hydrogen bonding contacts to GspB residue Tyr-485. In GspB, Tyr-443, Arg-484, and Tyr-485 have previously been investigated by site-directed mutagenesis and shown to be essential for carbohydrate binding. Arg-484 was further shown to be important for carbohydrate binding and virulence in an animal model of infective endocarditis (14), supporting the docking proposal.

The combination of these mutational studies with the $SrpA_{BR}$ cocrystal structure supports the Thr-Arg motif functioning to control the binding orientation of a sialic acid moiety. We propose that the Thr-Arg motif could be used to suggest plausible binding poses for carbohydrates in other members of the family by providing an anchoring orientation for one carbohydrate moiety. The resulting modeled ligands (di- or trisaccharides) in different adhesins can then be used to identify further residues that may contribute to selectivity and affinity.

Summary and Conclusions—The high resolution structure of $SrpA_{BR}$ both alone and in complex with a synthetic disaccharide identifies a sequence motif that binds and orients sialic acid. Moreover, this study suggests that closely related serine-rich repeat adhesins use short sequence insertions at key locations as one mechanism to modulate functional properties. It is

likely that these insertions are combined with amino acid substitutions to tune both structural and functional properties in this family.

Author Contributions—B. A. B. performed binding studies, mutagenesis, and data analysis. L. V. L. crystallized SrpABR, collected diffraction data, and performed dynamic light scattering. K. M. M. performed computational studies, assisted with data analysis and structure refinement, and made the figures. H. Y. synthesized the sialyl galactose disaccharide. K. R. V. designed constructs and developed purification protocols during the early stages of this project. S. A. and Z. W. processed diffraction data, calculated the initial phases, and performed the initial chain trace. X. C. guided the synthesis of sialyl galactose disaccharide. P. M. S. developed the experimental strategy, guided the study, and wrote the manuscript. T. M. I. designed the experimental strategy, guided the study, expressed and purified protein, refined the structures, and wrote the manuscript.

Acknowledgments—Use of the Advanced Photon Source, an Office of Science User Facility operated for the United States Department of Energy Office of Science by Argonne National Laboratory, was supported by the United States Department of Energy under Contract DE-AC02-06CH11357. Use of the LS-CAT Sector 21 was supported by the Michigan Economic Development Corp. and the Michigan Technology Tri-Corridor Grant 085P1000817.

References

1. Hoen, B., and Duval, X. (2013) Clinical practice. Infective endocarditis. *N. Engl. J. Med.* **368,** 1425–1433
2. Fitzgerald, J. R., Foster, T. J., and Cox, D. (2006) The interaction of bacterial pathogens with platelets. *Nat. Rev. Microbiol.* **4,** 445–457
3. Sullam, P. M., and Sande, M. A. (1992) Role of platelets in endocarditis: clues from von Willebrand disease. *J. Lab. Clin. Med.* **120,** 507–509
4. Murdoch, D. R., Corey, G. R., Hoen, B., Miró, J. M., Fowler, V. G., Jr., Bayer, A. S., Karchmer, A. W., Olaison, L., Pappas, P. A., Moreillon, P., Chambers, S. T., Chu, V. H., Falcó, V., Holland, D. J., Jones, P., *et al.* (2009) Clinical presentation, etiology, and outcome of infective endocarditis in the 21st century: the International Collaboration on Endocarditis-Prospective Cohort Study. *Arch. Intern. Med.* **169,** 463–473
5. Thornhill, M. H., Dayer, M. J., Forde, J. M., Corey, G. R., Chu, V. H., Couper, D. J., and Lockhart, P. B. (2011) Impact of the NICE guideline recommending cessation of antibiotic prophylaxis for prevention of infective endocarditis: before and after study. *BMJ* **342,** d2392
6. Tleyjeh, I. M., Steckelberg, J. M., Murad, H. S., Anavekar, N. S., Ghomrawi, H. M., Mirzoyev, Z., Moustafa, S. E., Hoskin, T. L., Mandrekar, J. N., Wilson, W. R., and Baddour, L. M. (2005) Temporal trends in infective endocarditis: a population-based study in Olmsted County, Minnesota. *JAMA* **293,** 3022–3028
7. Bensing, B. A., López, J. A., and Sullam, P. M. (2004) The *Streptococcus gordonii* surface proteins GspB and Hsa mediate binding to sialylated carbohydrate epitopes on the platelet membrane glycoprotein Ibα. *Infect. Immun.* **72,** 6528–6537
8. Plummer, C., Wu, H., Kerrigan, S. W., Meade, G., Cox, D., and Ian Douglas, C. W. (2005) A serine-rich glycoprotein of *Streptococcus sanguis* mediates adhesion to platelets via GPIb. *Br. J. Haematol.* **129,** 101–109
9. Takamatsu, D., Bensing, B. A., Cheng, H., Jarvis, G. A., Siboo, I. R., Lopez, J. A., Griffiss, J. M., and Sullam, P. M. (2005) Binding of the *Streptococcus gordonii* surface glycoproteins GspB and Hsa to specific carbohydrate structures on platelet membrane glycoprotein Ibα. *Mol. Microbiol.* **58,** 380–392
10. Deng, L., Bensing, B. A., Thamadilok, S., Yu, H., Lau, K., Chen, X., Ruhl, S., Sullam, P. M., and Varki, A. (2014) Oral streptococci utilize a Siglec-like domain of serine-rich repeat adhesins to preferentially target platelet sialoglycans in human blood. *PLoS Pathog.* **10,** e1004540
11. Takamatsu, D., Bensing, B. A., Prakobphol, A., Fisher, S. J., and Sullam, P. M. (2006) Binding of the streptococcal surface glycoproteins GspB and Hsa to human salivary proteins. *Infect. Immun.* **74,** 1933–1940
12. Xiong, Y. Q., Bensing, B. A., Bayer, A. S., Chambers, H. F., and Sullam, P. M. (2008) Role of the serine-rich surface glycoprotein GspB of *Streptococcus gordonii* in the pathogenesis of infective endocarditis. *Microb. Pathog.* **45,** 297–301
13. Turner, L. S., Kanamoto, T., Unoki, T., Munro, C. L., Wu, H., and Kitten, T. (2009) Comprehensive evaluation of *Streptococcus sanguinis* cell wall-anchored proteins in early infective endocarditis. *Infect. Immun.* **77,** 4966–4975
14. Pyburn, T. M., Bensing, B. A., Xiong, Y. Q., Melancon, B. J., Tomasiak, T. M., Ward, N. J., Yankovskaya, V., Oliver, K. M., Cecchini, G., Sulikowski, G. A., Tyska, M. J., Sullam, P. M., and Iverson, T. M. (2011) A structural model for binding of the serine-rich repeat adhesin GspB to host carbohydrate receptors. *PLoS Pathog.* **7,** e1002112
15. Pyburn, T. M., Yankovskaya, V., Bensing, B. A., Cecchini, G., Sullam, P. M., and Iverson, T. M. (2010) Purification, crystallization and preliminary x-ray diffraction analysis of the carbohydrate-binding region of the *Streptococcus gordonii* adhesin GspB. *Acta Crystallogr. Sect. F Struct. Biol. Cryst. Commun.* **66,** 1503–1507
16. Bensing, B. A., and Sullam, P. M. (2002) An accessory sec locus of *Streptococcus gordonii* is required for export of the surface protein GspB and for normal levels of binding to human platelets. *Mol. Microbiol.* **44,** 1081–1094
17. Otwinowski, Z., and Minor, W. (1997) Processing of x-ray diffraction data collected in oscillation mode. *Methods Enzymol.* **276,** 307–326
18. Winn, M. D., Ballard, C. C., Cowtan, K. D., Dodson, E. J., Emsley, P., Evans, P. R., Keegan, R. M., Krissinel, E. B., Leslie, A. G., McCoy, A., McNicholas, S. J., Murshudov, G. N., Pannu, N. S., Potterton, E. A., Powell, H. R., *et al.* (2011) Overview of the CCP4 suite and current developments. *Acta Crystallogr. D Biol. Crystallogr.* **67,** 235–242
19. Adams, P. D., Afonine, P. V., Bunkóczi, G., Chen, V. B., Davis, I. W., Echols, N., Headd, J. J., Hung, L. W., Kapral, G. J., Grosse-Kunstleve, R. W., McCoy, A. J., Moriarty, N. W., Oeffner, R., Read, R. J., Richardson, D. C., *et al.* (2010) PHENIX: a comprehensive Python-based system for macromolecular structure solution. *Acta Crystallogr. D Biol. Crystallogr.* **66,** 213–221
20. Terwilliger, T. C., Adams, P. D., Read, R. J., McCoy, A. J., Moriarty, N. W., Grosse-Kunstleve, R. W., Afonine, P. V., Zwart, P. H., and Hung, L. W. (2009) Decision-making in structure solution using Bayesian estimates of map quality: the PHENIX AutoSol wizard. *Acta Crystallogr. D Biol. Crystallogr.* **65,** 582–601
21. Cowtan, K. (2006) The Buccaneer software for automated model building. 1. Tracing protein chains. *Acta Crystallogr. D Biol. Crystallogr.* **62,** 1002–1011
22. Emsley, P., and Cowtan, K. (2004) Coot: model-building tools for molecular graphics. *Acta Crystallogr. D Biol. Crystallogr.* **60,** 2126–2132
23. Poornam, G. P., Matsumoto, A., Ishida, H., and Hayward, S. (2009) A method for the analysis of domain movements in large biomolecular complexes. *Proteins* **76,** 201–212
24. Ramboarina, S., Garnett, J. A., Zhou, M., Li, Y., Peng, Z., Taylor, J. D., Lee, W. C., Bodey, A., Murray, J. W., Alguel, Y., Bergeron, J., Bardiaux, B., Sawyer, E., Isaacson, R., Tagliaferri, C., *et al.* (2010) Structural insights into serine-rich fimbriae from Gram-positive bacteria. *J. Biol. Chem.* **285,** 32446–32457
25. Schulte, T., Löfling, J., Mikaelsson, C., Kikhney, A., Hentrich, K., Diamante, A., Ebel, C., Normark, S., Svergun, D., Henriques-Normark, B., and Achour, A. (2014) The basic keratin 10-binding domain of the virulence-associated pneumococcal serine-rich protein PsrP adopts a novel MSCRAMM fold. *Open Biol.* **4,** 130090
26. Seo, H. S., Xiong, Y. Q., and Sullam, P. M. (2013) Role of the serine-rich surface glycoprotein Srr1 of *Streptococcus agalactiae* in the pathogenesis of infective endocarditis. *PLoS ONE* **8,** e64204
27. Yang, Y. H., Jiang, Y. L., Zhang, J., Wang, L., Bai, X. H., Zhang, S. J., Ren, Y. M., Li, N., Zhang, Y. H., Zhang, Z., Gong, Q., Mei, Y., Xue, T., Zhang, J. R., Chen, Y., and Zhou, C. Z. (2014) Structural insights into SraP-mediated *Staphylococcus aureus* adhesion to host cells. *PLoS Pathog.* **10,**

e1004169
28. Sundaresan, R., Samen, U., and Ponnuraj, K. (2015) Structure of KRT4 binding domain of Srr-1 from *Streptococcus agalactiae* reveals a novel β-sheet complementation. *Int. J. Biol. Macromol.* **75,** 97–105
29. Yu, H., Chokhawala, H., Karpel, R., Yu, H., Wu, B., Zhang, J., Zhang, Y., Jia, Q., and Chen, X. (2005) A multifunctional *Pasteurella multocida* sialyltransferase: a powerful tool for the synthesis of sialoside libraries. *J. Am. Chem. Soc.* **127,** 17618–17619
30. Yu, H., Chokhawala, H. A., Huang, S., and Chen, X. (2006) One-pot three-enzyme chemoenzymatic approach to the synthesis of sialosides containing natural and non-natural functionalities. *Nat. Protoc.* **1,** 2485–2492
31. Li, Y., Yu, H., Cao, H., Lau, K., Muthana, S., Tiwari, V. K., Son, B., and Chen, X. (2008) *Pasteurella multocida* sialic acid aldolase: a promising biocatalyst. *Appl. Microbiol. Biotechnol.* **79,** 963–970
32. Yu, H., Yu, H., Karpel, R., and Chen, X. (2004) Chemoenzymatic synthesis of CMP-sialic acid derivatives by a one-pot two-enzyme system: comparison of substrate flexibility of three microbial CMP-sialic acid synthetases. *Bioorg. Med. Chem.* **12,** 6427–6435
33. Sugiarto, G., Lau, K., Qu, J., Li, Y., Lim, S., Mu, S., Ames, J. B., Fisher, A. J., and Chen, X. (2012) A sialyltransferase mutant with decreased donor hydrolysis and reduced sialidase activities for directly sialylating LewisX. *ACS Chem. Biol.* **7,** 1232–1240